

Supporting information for

Nanofibrous Aerogel Bulk Assembled by Crosslinked SiC/SiO_x Core-Shell

Nanofibers with Multifunctionality and Temperature-Invariant Hyperelasticity

Bo REN, Jingjing LIU, Yedong RONG, Lu WANG, Yuju LU, Xiaoqing XI, Jinlong*

*YANG**

State Key Laboratory of New Ceramics and Fine Processing, School of Materials

Science and Engineering, Tsinghua University, Beijing 100084, P. R. China

Corresponding authors. E-mail: ljtsinghua@126.com; jlyang@mail.tsinghua.edu.cn

Fabrication process of SCS-NAs.

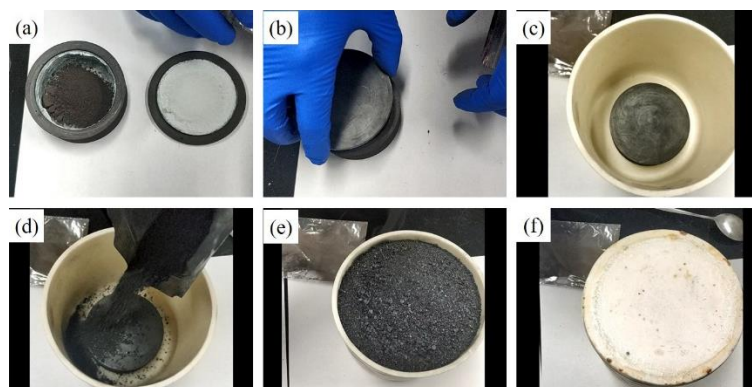


Figure S1 Fabrication process of SCS-NAs. (a) Silicon powder was placed into the graphite or alumina crucible; (b) the crucible was covered by a graphite/alumina lid as the template; (c) the small crucible was put inside a larger alumina crucible; (d-e) the small crucible was embedded with coke (the particle diameter was 1-0 mm); (f) the larger alumina crucible was covered by a lid before calcining at 1400 °C for 2 h.

Morphology of as-prepared SCS-NAs membrane and aerogel bulk. The experiment results confirmed that the SCS-NA membranes can be constructed onto an alumina or graphite template, as shown in Figure S2a,b. SiC particles and nanofibers can be observed at the bottom of the crucible (Figure S2c-d). After repeating CVD process for another 8 times, SCS-NAs bulk can be obtained (Figure S2e-f).

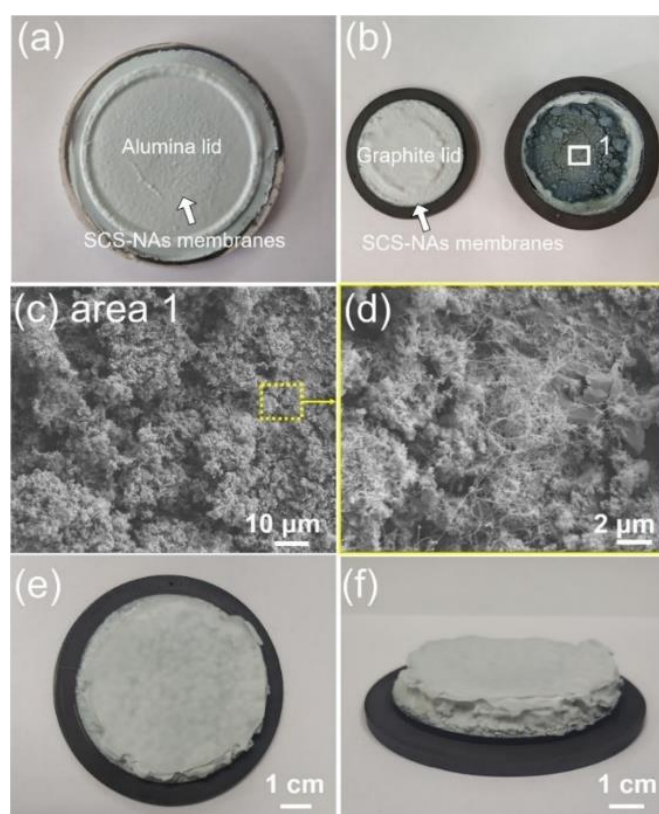


Figure S2 Digital photographs and microstructures of as-prepared products including SiC nanofibrous membrane, aerogel aerogels and SiC particles. After 1 cyclic preparation, SiC nanofibrous membrane can be deposited on (a) an alumina template or (b) graphite template, while the residual powder at the bottom became green, suggesting the formation of SiC; (c-d) Microstructure of the mixture at the bottom of crucible, demonstrating the formation of SiC particles and SiC nanofibers; (e-f) SiC nanofibrous aerogels obtained after another 8 cycles of layer-by-layer self-assembly.



Figure S3 Thickness, diameter, and the weight of as-prepared SCS-NAs bulk.

The presence of the Si and O element confirmed the deposition of SiO_x on the surface of nanofibers and junctions. By comparison, the mass ratio of O element for the fiber-to-fiber junction (37.00wt%) was much higher than that of nanofiber (6.47wt%), which was attributed to the deposition of a large amount of $\text{SiO}(\text{g})$.

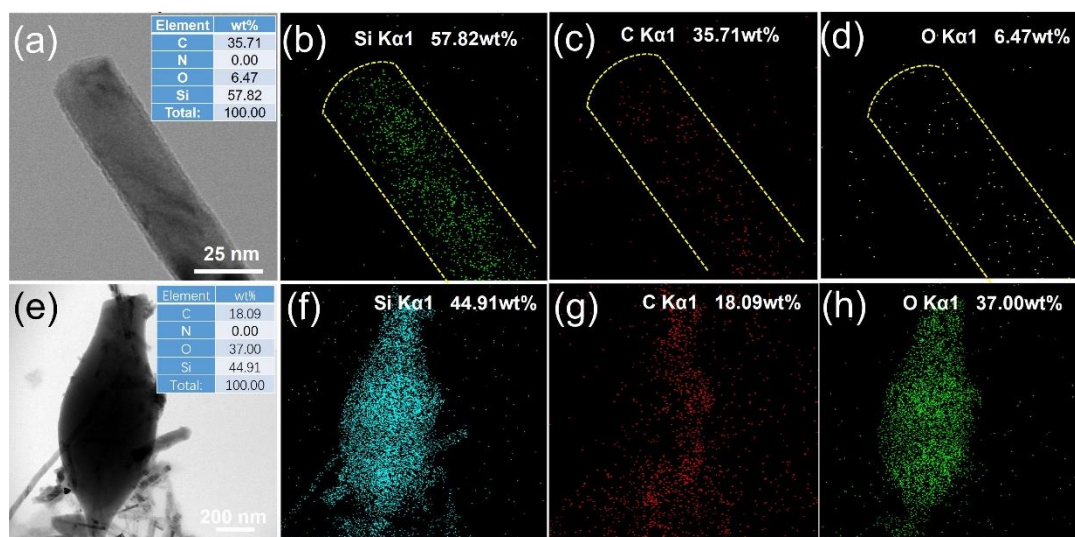


Figure S4 EDS results of a single core-shell nanofiber and the crosslinking: (a-d) a single SiC/SiO_x core-shell nanofiber; (e-h) fiber-to-fiber junction.

1000 loading-unloading fatigue cycles of SCS-NAs in liquid nitrogen

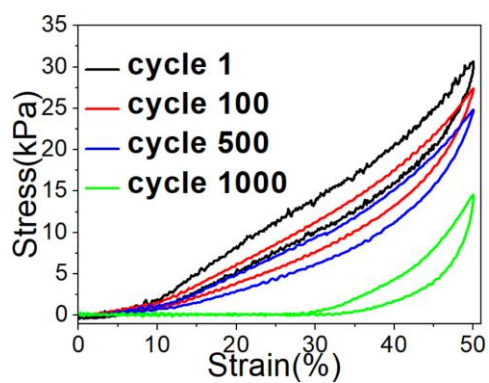


Figure S5 1000 loading-unloading fatigue cycles of SCS-NAs with 50% ϵ after immersing in liquid nitrogen directly

TGA analysis and microstructure of various SiC nanofibers.

Figure S6a showed the microstructure of as-prepared SiC/SiO_x core-shell nanofiber with a fiber diameter of 20~50 nm; Figure S6b demonstrated the commercial SiC nanofiber purchased from XFNANO Co., Ltd., China, with a fiber diameter over 100 nm; Figure S6c displayed the commercial SiC nanofiber/whisker purchased from Alfa Aesar Co., Ltd., USA, with a fiber diameter of 100~1000 nm. Apparently, the commercial SiC nanofibers were much coarser than ours. TG curves of various SiC nanofibers are shown in Figure S6d. As for the SiC/SiO_x core-shell nanofibers, a total mass loss of 2.25 wt% before 800 °C can be detected, which was attributed to the water evaporation and oxidation of carbonaceous substance.¹ In contrast to the commercial nanofibers with relatively fast oxidation behaviors, the well-adhered SiO_x shell could prevent the SiC core from fast oxidation, resulting in a small slope at 800~1100 °C. The oxidation temperature (the maximum temperature at $d_{\text{weight}}/d_{\text{temperature}}=0$ in the curves) of SCS-NAs was comparable to that of commercial SiC nanofibers with larger fiber diameters, suggesting its enhanced oxidation resistance.

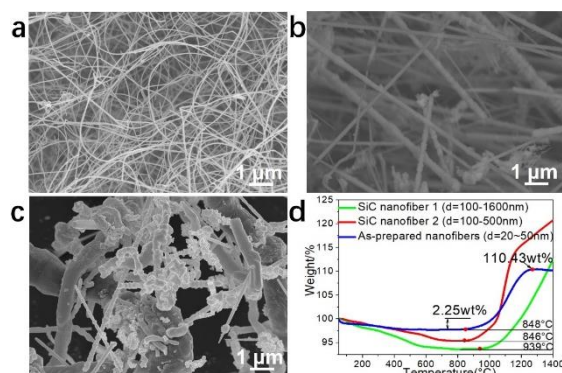


Figure S6 Microstructure of (a) as-prepared SiC/SiO_x core-shell nanofibers and (b-c) two kinds of commercial SiC nanofibers. (d) TGA analysis of various SiC nanofibers.

Hyperelasticity of 1100-SCS-NAs. 1100-SCS-NAs were also subjected to a fatigue hysteresis test for 1000 compressive cycles at a large compressive strain (ϵ) of 50% with a constant loading speed of 150 mm min⁻¹. Figure S6 demonstrated that no significant decrease in the maximum stress and Young's modulus can be detected after 100 loading-unloading fatigue cycles.

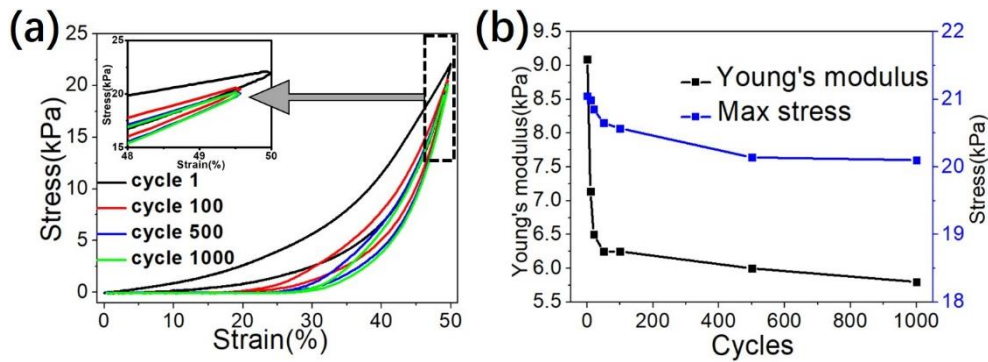


Figure S7. Mechanical properties of 1100-SCS-NAs (a) 1000 loading-unloading fatigue cycles of SCS-NAs with 50% ϵ . (b) The maximum stress and Young's modulus at different compressive cycles.

Specific BET Surface Area of the SCS-NAs. The high Brunauer-Emmett-Teller (BET) surface area ($142 \text{ m}^2 \text{ g}^{-1}$) of SCS-NAs was confirmed by N_2 adsorption-desorption isotherms, endowing them with a promising ability for separating various PMs.

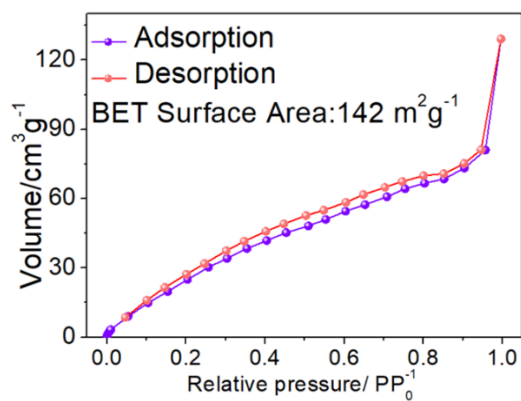


Figure S8 N_2 adsorption-desorption isotherm of SCS-NAs.

XPS spectra of incense smoke

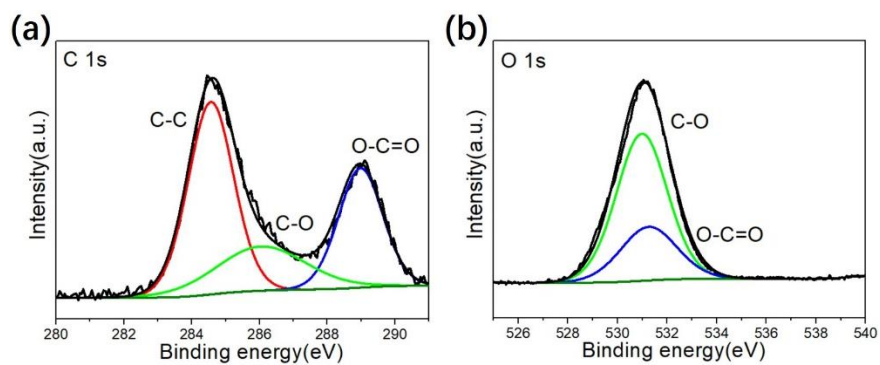


Figure S9 XPS spectra of incense smoke, demonstrating the main groups of C-C, O-C=O and C-O in (a) C 1s and (b) O 1s characteristic peaks.

Surface modification of SCS-NAs. The wettability of SCS-NAs can transform from hydrophilicity to hydrophobicity by the surface modification method. The pristine SCS-NAs exhibited superhydrophilicity with a water contact angle (WCA) of $\sim 5^\circ$ (Figure S10 a). By comparison, surface-modified SCS-NAs were highly hydrophobic with a WCA of $\sim 143^\circ$, which was crucial for the collection of oils and organic solvents (Figure S10 b). It is also demonstrated that a piece of surface-modified SCS-NAs membrane can support a water droplet on its surface (Figure S10 c).

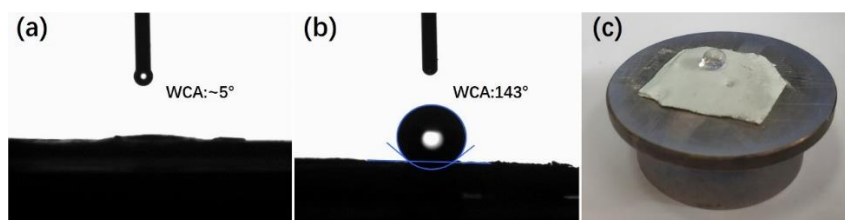


Figure S10 Water contact angles of (a) pristine and (b) surface-modified SCS-NAs.

(c) a water drop on the surface of modified SCS-NAs

Supplementary Discussion

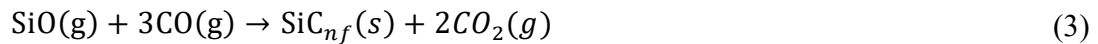
Thermodynamics analysis for the formation mechanism of SCS-NAs. The atmosphere created by the coke bed contains approximate 0.35 atm CO(g) and 0.65 atm N₂(g) at high temperature. At high temperature, the diffusion of CO(g) and N₂(g) enables the formation of SCS-NAs and SiC particles. Among these reactions, Eq (1) and (2) occur preferentially from the perspective of both thermodynamics and kinetics. These reactions lead to the persistent generation of SiC nanofibers and particles, along with a larger amount of CO₂(g). It should be noted that the partial pressure of CO(g) is assumed to be stabilized at 0.35 atm during the thermodynamic calculations. It is also demonstrated that at 1673K (1400 °C), Eq(3) can take place with a CO₂(g) partial pressure less than 6.23×10⁻⁴ atm, which in fact would not proceed as a consequence of a high CO₂(g) partial pressure caused by Eqs(1-2). Thus, most of the SiO(g) would deposit randomly onto the surface of SiC nanofibrous network to form core-shell structure and crosslinking.



$$\Delta G_1 = G_1^\theta + RT \ln \frac{p_{\text{co}_2}/p^\theta}{(p_{\text{co}}/p^\theta)^2}$$



$$\Delta G_2 = G_2^\theta + RT \ln \frac{p_{\text{co}_2}/p^\theta}{(p_{\text{co}}/p^\theta)^2}$$



$$\Delta G_3 = G_3^\theta + RT \ln \frac{(p_{\text{co}_2})^2}{(p_{\text{co}}/p^\theta)^3}$$



Supplementary Methods

Surface modification of SCS-NAs. Before modification, SCS-NAs were ultrasonically washed in deionized water and ethanol for 20 min, respectively. After cleaning, they were dried in the oven at 80 °C for 24 h. The dried SCS-NAs were immersed in a 1.0 vol% *n*-heptane solution of OTS for 1 h at room temperature. After etching, the samples were rinsed with ethanol and dried at 100 °C in the vacuum for 6 h.

Density and porosity measurement of SCS-NAs and 1100-SCS-NAs. In the current work, the apparent densities of the nanofibrous aerogels were obtained based on the ISO 845:2006 standard by the following equation:

$$\rho = \frac{m}{V}$$

where m and V stand for the mass of solid constituents and volume of the aerogel bulk, respectively; ρ is the apparent density of the aerogel bulk.

The porosity of aerogel bulk was determined according to its apparent density and the density of the solid constituents by the following formula:

$$V = \left(1 - \frac{\rho}{\rho_0}\right) \times 100\%$$

where ρ and ρ_0 are the apparent and theoretical densities, respectively.

In the current case, SCS-NAs with an ultralow density of $\sim 23 \text{ mg cm}^{-3}$, the solid constituents are the SiC/SiO_x nanofibers, which have a density of about 3.21 g cm^{-3} , corresponding to a porosity of 99.3%.

After calcining at $1100 \text{ }^\circ\text{C}$, the aerogel bulk constructed by the amorphous SiO₂ nanofibers was obtained with a density of $\sim 25 \text{ mg cm}^{-3}$, yielding a porosity of 98.9%. (the density of solid constituents is 2.2 g cm^{-3} according to the previous work.² The porosity of 1100-SCS-NAs was a bit lower than that of SCS-NAs because of the volume expansion during the oxidation of SiC nanofibers.

Temperature-invariant hyperelasticity of SCS-NAs. The hyperelasticity of SCS-NAs was performed at various temperatures ranging from -196°C to -10°C using ethanol/liquid nitrogen (-116°C , approximately), acetone/liquid nitrogen (-95°C , approximately), ethanol/dry ice (-72°C , approximately), *n*-octane/dry ice (-56°C , approximately), and ethanediol/dry ice (-10°C , approximately) baths to create low temperatures. For the preparation of these baths, the dry ice or liquid nitrogen was added into the organic solvents gradually until the latter started to solidify. The compressive tests can be finished within 10 s. During the test, the sample did not contact with the low-temperature organic solvent directly because their hyperelasticity could change after absorbing the organics.

References

- (1) Su, L.; Wang, H.; Niu, M.; Fan, X.; Ma, M.; Shi, Z.; Guo, S. Ultralight, Recoverable, and High-Temperature-Resistant SiC Nanowire Aerogel. *ACS Nano* **2018**, *12*, 3103–3111.
- (2) Si, Y.; Wang, X.; Dou, L.; Yu, J.; Ding, B. Ultralight and Fire-Resistant Ceramic Nanofibrous Aerogels with Temperature-Invariant Superelasticity. *Sci. Adv.* **2018**, *4*, eaas8925.